Available online at www.sciencedirect.com
ScienceDirect
International Journal of Heat and Fluid Flow 28 (2007) 787–805
International Journal of HEAT AND FLUID FLOW
www.elsevier.com/locate/ijhff

A numerical investigation and parametric study of cooling an array of multiple protruding heat sources by a laminar slot air jet

E. Arquis [a], M.A. Rady [b,1], S.A. Nada [b,*]

[a] TREFLE-UMR CNRS 8508, Site ENSCPB, University Bordeaux I, 16 Avenue Pey Berland, F33607 Pessac Cedex, France
[b] Department of Mechanical Engineering Technology, Benha High Institute of Technology, Benha 13512, Egypt

Received 3 October 2005; received in revised form 10 July 2006; accepted 12 September 2006
Available online 22 November 2006

Abstract

The present article reports on the fluid flow and heat transfer characteristics associated with cooling an in-line array of discrete protruding heated blocks in a channel by using a single laminar slot air jet. Numerical experiments have been carried out for different values of jet Reynolds number, channel height, slot width, spacing between blocks, block height, and block thermal conductivity. The effects of variation of these parameters are detailed to illustrate important fundamental and practical results that are relevant to the thermal management of electronic packages. In general, the effective cooling of blocks has been observed to increase with the increase of Reynolds number and the decrease of channel height. Heat transfer rates are enhanced for shorter and widely spaced heated blocks. Circulation cells that may appear on the top surface of the downstream blocks have been shown to decrease the value of Nusselt number for these blocks. The values of surface averaged Nusselt number attain their maximum at the block just underneath the impinging air jet, decrease for the downstream blocks, and approximately reach a constant value after the third block. Useful design correlations have been obtained for the mean Nusselt number for the heated blocks underneath and downstream the impinging jet.

Keywords: Electronics cooling; Multiple heat sources; Laminar; Slot jet

1. Introduction

Because of their high heat removal rates, impinging jets are widely used for heating, cooling and drying in several industrial applications. They have been also considered for use in electronics cooling and, in particular, for chip arrays characterized by large power dissipation. Unique features of such an application include the existence of discrete heat sources, confinement of the jet in a channel formed by a surface that is connected to the jet exit and parallel to the impingement surface (due to packaging constraints), and preference for using laminar rectangular jets to cool multiple heat sources (to minimize overall flow requirements and to meet the limitation of the resulting force of air jet exerted on the package). As compared to round jets, the use of two-dimensional or planar air jets can offer some beneficial features, such as cooling effectiveness, uniformity and controllability (Wadsworth and Mudawar, 1990; Lin et al., 1997). The present study is motivated by such an application, and its specific purpose is to numerically determine flow and heat transfer phenomena associated with using a confined laminar slot jet to cool a linear array of protruding discrete heat sources. The fundamental basis of the present study are related to fluid flow and heat transfer phenomena around bluff bodies and jet impingement cooling of protruding heat sources. These configurations are briefly discussed in the following paragraphs with reference to the most recent literature reviews.

The fluid flow in a channel containing multiple protruding heated obstacles has been of interest for several decades as the canonical model for electronic components cooling. Both numerical and experimental methods have been employed as detailed by Incropera (1988), Peterson and

* Corresponding author. Tel.: +20 105026895; fax: +20 133230297.
E-mail address: samehnadar@yahoo.com (S.A. Nada).
[1] Currently visiting professor at TREFLE.

0142-727X/$ - see front matter © 2006 Elsevier Inc. All rights reserved.
doi:10.1016/j.ijheatfluidflow.2006.09.004

Nomenclature

A	exposed surface area of the block, m^2
a	block height, m
B	slot width, m
c	specific heat, J/kg K
Da	Darcy number, K/B^2
H	channel height, m
h	heat transfer coefficient, W/m^2 K
K	permeability, m^2
k	thermal conductivity, W/m K
L	block length, m
L_e	distance between the last block and the channel exit, m
N	block number, dimensionless
Nu	local Nusselt number, dimensionless
$\overline{NU}$	block surface averaged Nusselt number, dimensionless
n	unit vector normal to block surface, dimensionless
P	pressure, N/m^2
p	dimensionless pressure, $P/\rho V_j^2$
Pr	Prandtl number, v/α
q'''	heat dissipation density $= Q/(a_s \cdot L)$, W/m^3
Re	Reynolds number, $V_j B/v$
S	spacing between blocks, m
T	temperature, °C
T_j	jet inlet temperature, °C
T_s	block surface temperature, °C
t	time, s
V_j	jet exit velocity, m/s
U, V	velocity components in X and Y directions, m/s
u, v	dimensionless velocity components in x and y directions (U/V_j, V/V_j)
X, Y	Cartesian coordinates, m
x, y	dimensionless coordinates (X/B, Y/B)
α	thermal diffusivity, m^2/s
v	kinematic viscosity, m^2/s
ρ	density, kg/m^3
τ	dimensionless time, tV_j/B
θ	dimensionless temperature $(T - T_j)/(Q/k_f)$

subscripts

a	air
b	block
f	fluid
j	jet
s	block surface

Ortega (1990) and Kim and Lee (1996). In most investigations, the problem is idealized to the fluid flow and thermal analysis of heat generating quadrilateral obstacles, representing the electronic devices, within a parallel plate channel for different entry flow conditions and obstacle geometry. This description of the problem allows general results to be obtained in lieu of system specific results. An extensive numerical investigation of forced convection cooling of an array of inline heated obstacles in a two-dimensional channel has been recently presented by Young and Vafai (1998). The dependence of the streamlines, isotherms, and Nusselt number on the governing parameters has been documented. It has been shown that specific choices in certain governing parameters, such as obstacle height or spacing, can make significant changes in the cooling of obstacles.

On the other hand, the most recent reviews on jet impingement by Plot et al. (1989), Jambunathan et al. (1992) and Yeh (1995), among others, show that relatively few work have been performed for cooling an array of multiple heat sources. An experimental study has been carried out by Wadsworth and Mudawar (1990) to investigate the heat transfer from a 3×3 array of simulated chips by using dielectric liquid slot jets impinging on each chip. The effects of slot width, height of the confinement, and the liquid Reynolds number on the convection heat transfer coefficient have been examined. The cooling performance of a uniform array of modules, using four round air jets for each module in a semi-confined arrangement, has been experimentally investigated by Hollworth and Durbin (1992).

Studies on cooling multiple heat sources using a single jet are very few. Conjugate convection/conduction numerical simulations of laminar air jet convective heat transfer from discrete heat sources flush mounted in a flat plate and a flat disc have been conducted by Schafer et al. (1992) and Bula et al. (2000), respectively. The effects of jet velocity profiles and pertinent dimensionless parameters on flow and heat transfer conditions have been calculated. An experimental study to analyze the thermal wake effect during single slot jet impingement cooling of multiple in-line protruding heat sources has been carried out by Huzyyien et al. (2006). Correlations have been derived for the thermal wake function and a superposition technique has been employed to estimate the source temperature. Numerical and experimental studies of local heat transfer of impinging turbulent gas jets on a cylindrical pedestal have been reported by Mesbah (1996) and Behnia et al. (1999). The presence of a minimum heat transfer coefficient at the stagnation point, instead for a maximum for the flat plate, emphasizes the need for CFD simulations in more complex geometries, Behnia et al. (1999).

To the best of the authors' knowledge, no detailed analysis has been performed for fluid flow and heat transfer characteristics during jet impingement cooling of an in-line array of protruding heat sources simulating electronic components. In the present study, numerical investigations of cooling an in-line array of multiple protruding heated blocks by a single laminar slot air jet have been conducted. Numerical experiments have been carried out for different

values of jet Reynolds number (Re), dimensionless channel height (H/L), dimensionless slot width (B/L), ratio of block spacing to block length (S/L), ratio of block height to block length (a/L), and ratio of block thermal conductivity to fluid thermal conductivity (k_b/k_f). The effects of these parameters on the fluid flow and heat transfer characteristics are identified and understood. Extensive presentation and evaluation of the surface averaged and local distribution of Nusselt number for all the blocks of the array are fully documented.

2. Physical model

The configuration of the problem under investigation is shown in Fig. 1(a). It describes an impinging jet flow normal to a critical block of an inline multiple heated blocks mounted on the bottom plate of a channel. The jet exits through a slot of width B at distance H from the bottom plate. Multiple heated blocks of length L, height a, and spacing S are fixed on the bottom plate. The flow exits the channel at distance L_e beyond the last heated block. The geometry is defined such that the blocks and the horizontal plates are continuous in the third dimension. For a PC board, IC components are generally arranged in rows in such a way that the spacing between components in each row is small compared to the spacing between the rows. Also, the length of each row (length or width of the PC board) is at least one order of magnitude higher than the width of each component. Therefore, the two-dimensional model for the flow and temperature fields provides a good approximation.

In practice, the thermal energy release in each block is located in a very thin layer in the bottom of the block where the IC exists. However, in the previous investigations, this has been approximated as a constant surface heat flux input at the block base or as a uniform volumetric heat generation inside the whole body of the block. Young and Vafai (1998) numerically studied the effects of the two approaches on the isotherms for different values of block to fluid thermal conductivity ratio k_b/k_f. The two approaches have been shown to give different isotherms around the heated blocks. The differences have been noticed to vanish with increasing k_b/k_f. In the present study, in order to simulate the actual case of electronic components, the thermal energy release in each block is considered as a uniform volumetric heat generation q''' in a thin layer of thickness a_s and length L in the bottom of each block, $a_s/L = 0.0125$. The bottom and top plates of the channel are assumed adiabatic.

3. Mathematical formulation

Mathematical formulation of the present problem are based on two-dimensional, steady, laminar, and incompressible flow with constant properties and negligible buoyancy effects, $Gr/Re^2 \ll 1$. The dimensionless governing equations for mass, momentum and energy are obtained using the jet width B, the jet exit velocity V_j, the jet exit temperature T_j, and the characteristics pressure ρV_j^2 as scaling parameters for length, velocity, temperature, and pressure, respectively. They are written in general form for the whole computational domain as

$$\frac{\partial u}{\partial x}+\frac{\partial v}{\partial y}=0 \tag{1}$$

$$\frac{\partial u}{\partial \tau}+u\frac{\partial u}{\partial x}+v\frac{\partial u}{\partial y}=-\frac{\partial p}{\partial x}+\frac{1}{Re}\left(\frac{\partial^2 u}{\partial x^2}+\frac{\partial^2 u}{\partial y^2}\right)-\frac{u}{DaRe} \tag{2}$$

$$\frac{\partial v}{\partial \tau}+u\frac{\partial v}{\partial x}+v\frac{\partial v}{\partial y}=-\frac{\partial p}{\partial y}+\frac{1}{Re}\left(\frac{\partial^2 v}{\partial x^2}+\frac{\partial^2 v}{\partial y^2}\right)-\frac{v}{DaRe} \tag{3}$$

$$\frac{\partial \theta}{\partial \tau}+u\frac{\partial \theta}{\partial x}+v\frac{\partial \theta}{\partial y}=\frac{k^*}{Re\cdot Prc^*}\left(\frac{\partial^2 \theta}{\partial x^2}+\frac{\partial^2 \theta}{\partial y^2}\right)+\frac{1}{RePrc^*}\frac{1}{a_s^* l^*}f(\Omega) \tag{4}$$

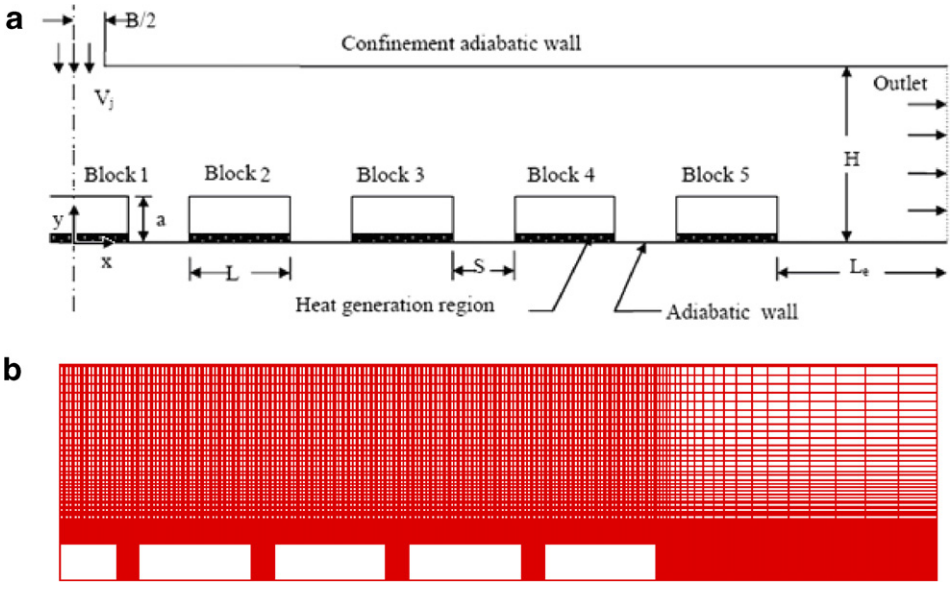

Fig. 1. Physical model (b) and computational grid (b).

where

$$u = U/V_j, \quad v = V/V_j, \quad \tau = tV_j/B, \quad x = X/B,$$
$$y = Y/B, \quad p = P/\rho V_j^2, \quad Re = V_j B/\nu, \quad Pr = \nu/\alpha,$$
$$k^* = k_b/k_f, \quad c^* = (\rho c)_b/(\rho c)_f, \quad a_s^* = a_s/B,$$
$$l^* = L/B, \quad \text{and} \quad \theta = T - T_j/(Q/k_f)$$

It should be observed that, the third term on the right hand-side of the momentum equations, Eqs. (2) and (3), represents the Darcy drag force that is well known for modeling fluid flow in porous media. This term is introduced here to accommodate the presence of solid block protrusions within the whole domain. The solid blocks are treated as a porous media with a very low permeability ($K = 10^{-30}$ m^2) in comparison with the infinite permeability of the surrounding fluid ($K = 10^{30}$ m^2). The low value of the permeability in the solid region ensures an impermeable condition with zero velocity. This technique is similar to the blocking-off method introduced by Patankar (1980) to handle conjugate heat transfer problems. The present method is mathematically classified as one of the penalty methods used to treat porous and solid obstacles using single-domain modeling approaches. The penalization term that is adopted in the present formulation makes use of the very low permeability value to force the velocity to zero in the solid regions (Arquis and Caltagirone, 1984; Angot et al., 1999; Khadra et al., 2000). In the energy equation $f(\Omega)$ is a step function which is set to zero everywhere except in the heat dissipation region at the bottom of each block (thickness a_s and width L). In the fluid regions, k^* and c^* are set equal to one. In the solid block regions, depending on the thermal properties of the block material, k^* and c^* are different from one. However, since the solid velocity is identically zero, the effect of c^* on the steady state results is eliminated and c^* can be set equal to one for the whole domain. The adoption of the present methodology requires no explicit boundary conditions to be specified at the fluid–solid interface. Thus the boundary conditions for both the velocity and temperature fields can easily be supplied at the outer surfaces of the calculation domain.

In the present study, the fluid exits the slot with a uniform temperature and velocity (T_j, V_j). The top (excluding the slot jet width) and bottom walls of the computational domain have been considered impermeable and adiabatic surfaces. Because of the symmetry, it is sufficient to consider only one-half of the flow field as shown in Fig. 1 (a). Outflow boundary condition has been employed on the right boundary of the computational domain. These boundary conditions can be expressed mathematically in dimensionless form as follows:

(1) Slot exit: $u = 0$, $v = 1$ and $\theta = 0$
(2) Channel outflow: $\frac{\partial u}{\partial x} = 0$, $\frac{\partial v}{\partial x} = 0$, $\frac{\partial \theta}{\partial x} = 0$
(3) Channel top wall excluding the slot jet entry width: $u = 0$, $v = 0$, $\frac{\partial \theta}{\partial y} = 0$
(4) Symmetry axis: $u = 0$, $\frac{\partial v}{\partial x} = 0$, $\frac{\partial \theta}{\partial x} = 0$
(5) Channel bottom wall $u = 0$, $v = 0$, $\frac{\partial \theta}{\partial y} = 0$

It is important that the conditions imposed at the outlet boundary do sufficiently match the assumed outflow boundary condition, zero gradient. The proper location of the outlet boundary (L_e) depends on the flow situation and is determined by numerical experiments. A calculation domain size of $L_e = 12L$ has been found to be satisfactory for all the range of parameters studied. Re-locating the outflow boundary further away does not affect the solution in the heated blocks and jet impingement regions.

According to the definition of Newton's law of cooling, the local convective heat transfer coefficient at the surface of the heated block can be expressed in terms of the fluid temperature gradient at the solid–fluid interface as

$$h\theta_s = -\frac{k_f}{B}\frac{\partial \theta}{\partial n}\bigg|_s \tag{5}$$

where n is the outward normal to the block surface at the solid–fluid interface, dimensionless, i.e. $n = y$ for the top face of the block and $n = x$ at the left and right faces of the blocks.

Thus the local Nusselt number, based on block length, along the surface of the blocks is calculated using:

$$Nu = \frac{hL}{k_f} = -\frac{L}{B}\frac{1}{\theta_s}\frac{\partial \theta}{\partial n}\bigg|_s \tag{6}$$

The surface averaged Nusselt number for each block is calculated as follows:

$$\overline{Nu} = \frac{1}{A}\int_A Nu \, dA \tag{7}$$

The right, left, top, and overall surface averaged Nusselt number for each block is obtained by integrating Eq. (7) over the corresponding value of surface area.

4. Numerical solution and validations

The governing equations have been discritized using the control volume based finite difference formulation with implicit time integration (Patankar, 1980). The computational domain has been divided into a large number of control volumes. The grid is designed such that the surfaces of solid blocks coincide with the control volumes faces. This allows appropriate assignment of the values of density, specific heat, viscosity, thermal conductivity, and permeability at the central nodes of both the solid and fluid computational cells. The diffusion coefficients (viscosity and thermal conductivity) at the faces of the control volumes have been calculated as the harmonic mean of their respective known values at the central nodes. The adoption of harmonic mean practice ensures the continuity of diffusive fluxes at the control volume faces and correctly handles the large step change in the diffusion coefficients at the solid–liquid interface (Patankar, 1980).

Solution of Navier–Stokes equations has been carried out using the augmented Lagrangian method (Fortin and

Glowinski, 1982). This iterative method consists of solving an optimization problem to search for a velocity–pressure saddle point under the constraint of incompressibility ($\Delta \cdot \vec{V} = 0$) by using an Uzawa algorithm. Starting with an initial pressure field, the Navier–Stokes equations, modified with the introduction of the incompressibility constraint, are solved for the velocity field. A new pressure field is then calculated using a modified equation of continuity. The iterations of the augmented Lagrangian method are repeated until a numerical threshold controlling the compressibility constraint is reached. Since the pressure field is calculated directly from the velocity field, no boundary conditions are needed for the pressure.

Hybrid scheme has been chosen for discretization of the convective–diffusive transport terms. The discrete algebraic equations have been solved using a preconditioned conjugate gradient method BI-CGSTAB. Steady state numerical solution has been obtained by retaining the transient terms in the governing equation. This technique provides a kind of under-relaxation and improves the convergence to steady state solution (Patankar, 1980). Calculations are terminated, steady state is considered satisfied, when the normalized difference in the values of temperatures and velocities between two successive iterations in time are less than 10^{-10}. The value of the normalized mass imbalance, residual of continuity equation, is less than 10^{-12}. These criteria have been found sufficient to ensure accurate results of steady state temperature and velocity fields. The difference in the Nusselt number value between two successive iterations at steady state is less than 10^{-6}.

To validate the numerical model and scheme used in the present study, comparisons with previous studies have been performed. This has been accomplished through adjustments to the model to match the geometric, hydrodynamic, and thermal conditions of the related works. Since the present problem includes laminar jet impingement on protruding heated blocks, it would be useful to verify the present model against experimental and or numerical data for jet impingement on a single protruding object or pedestal. However, the numerical and experimental data available in the literature for such configuration are limited to turbulent flow (Behnia et al., 1999). In order to avoid this difficulty and assure the accuracy of the present code to treat similar configurations, comparisons have been made with the numerical published results of Young and Vafai (1998) for laminar forced convection cooling of single and multiple heated blocks in a channel. The predicted streamlines and isotherms plots agree with Young and Vafai (1998) solution. In particular, the current calculations found similar boundary layer development along the upper surface of the blocks and correctly capture the development of upstream, inter-block, and downstream recirculation cells as reported by Young and Vafai (1998). For jet impingement configurations, comparisons have been made with the experimental results of Sparrow and Wong (1975) for laminar free slot air jet impinging on a flat plate. The experiments have been performed with jets that are laminar at the exit of the duct from which the jet issues. The computational domain corresponding to Sparrow and Wong experiments includes both the jet duct and impingement surface in order to avoid any assumptions regarding velocity profile at the jet exit, see Fig. 2a. Because of symmetry, one half of the physical domain is considered for numerical computation using a 120×120 non-uniform grid. It can be observed from Fig. 2b that the agreement between the present predicted local distribution of heat transfer Nusselt number and the experimental measurements is good. Further validations have been performed by comparison with the experimental work of Lin et al. (1997) for semi-confined laminar slot jet impingement on a flat plate. As shown in Table 1, the present model predicts the experimental results with an error of 3% that lies within the uncertainty range of the experiments. In

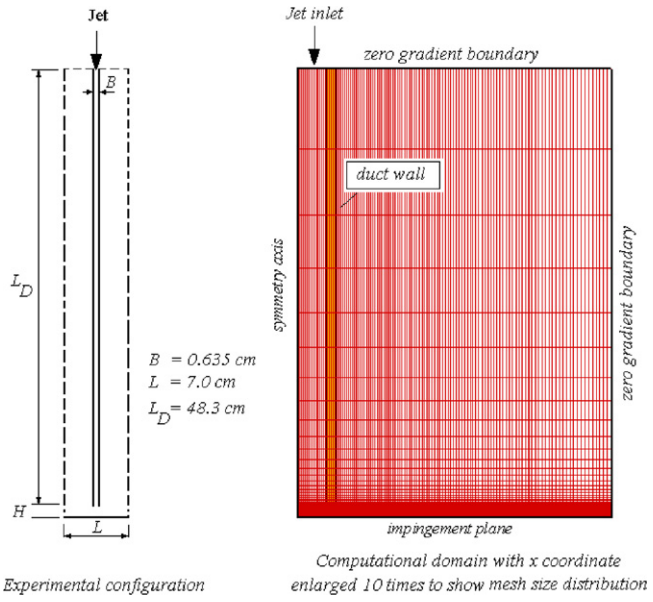

Fig. 2a. Experimental configuration and computational domain for Sparrow and Wong (1975) experiments.

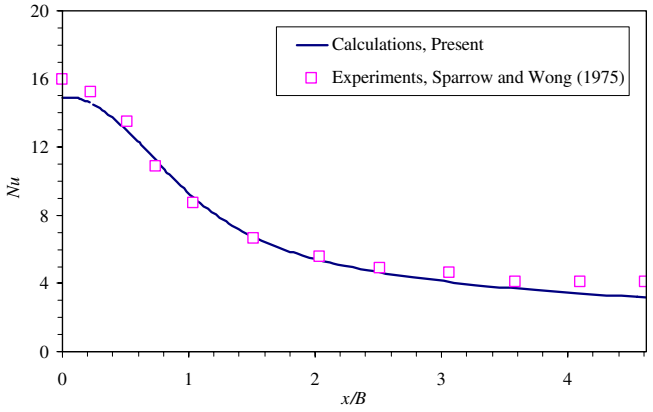

Fig. 2b. Comparison of the local Nusselt number with experimental data of Sparrow and Wong (1975) ($Re = 450$, $H/B = 2$).

Table 1
Comparison of the present results of stagnation Nusselt number with the experimental results of Lin et al. (1997) ($H/B = 4$)

Re	$Nu_{stagnation}$	
	Lin et al. (1997)	Present
100	6.44	6.272
200	9.10	8.97
400	12.88	12.81

addition to the above mentioned validations, the present code has been validated for many other standard academic reference cases, Aquilon (2006).

For the present problem configuration, extensive grid refinement study has been carried out to determine the effect of grid size (identified by N and M control volumes in the x and y directions, respectively) on the accuracy of the numerical solution and insure grid independent results. Fig. 1(b) shows a typical non-uniform mesh employed for the present calculations. Grid points are highly concentrated at the block/fluid interfacial boundaries to provide sufficient mesh density without elements distortion and to capture the critical features near the block region. The impact of grid size on the steady state average value of Nusselt number for the different blocks of the array is shown in Table 2 for a typical test run having $Re = 500$, $H/L = 0.75$, $B/L = 0.5$, $S/L = 0.1$, $a/L = 0.5$, $k_b/k_f = 10$ and $Pr = 0.7$. It can be observed that, the differences in the calculated value of the mean Nusselt number for the different blocks of the array using 167×60 and 216×60 grid systems are less than 0.6%. Thus a grid system having $N = 216$ nodes in the x direction is sufficient to produce accurate results. The effect of grid refinement in the y direction is also shown in Table 2. The differences in the calculated value of the mean Nusselt number for the different blocks of the array using 216×80 and 216×100 grid systems are less than 0.6%. Based on this grid refinement study, the results obtained using 216×100 can be considered as grid independent. This grid has been employed in all the numerical simulations of the present results. The results of additional calculations obtained using 432×200 grid, also shown in Table 2, show negligible differences as compared to the results obtained using 216×100 grid.

Table 2
Effect of grid size on the average Nusselt number for different blocks of the array

Block number	Grid ($M \times N$)					
	118×60	167×60	216×60	216×80	216×100	432×200
1	13.494	13.660	13.601	13.045	12.980	12.935
2	8.068	7.948	7.970	7.743	7.709	7.733
3	4.687	4.636	4.580	4.539	4.522	4.481
4	3.859	3.845	3.823	3.791	3.782	3.770
5	3.458	3.454	3.441	3.412	3.407	3.400

$Re = 500$, $H/L = 0.75$, $B/L = 0.5$, $S/L = 0.1$, $a/L = 0.5$, $k_b/k_f = 10$, $Pr = 0.7$.

5. Results and discussion

Numerical experiments have been carried out using air $Pr = 0.70$, for different values of Reynolds number $Re = (100, 200, 300, 400, 500)$, channel height to heated block length $H/L = (0.5, 0.75, 1)$, slot width to block length $B/L = (0.25, 0.5, 1.0)$, block height to block length $a/L = (0.0627, 0.125, 0.25)$, and block thermal conductivity $k_b/k_f = (10, 100, 1000)$. The parameters describing the geometry of the present array are representative of typical parameters encountered in electronics cooling applications (Kim and Lee, 1996). They correspond to a packing density $\{L/(L + S)\}$ in the range of 0.5–0.9 and package profile ratio in the range 0.714-1. The values of k_b/k_f represent typical materials utilized in electronic packaging, such as epoxy glass, ceramic and heat spreaders. It should be mentioned that this range of flow parameters is consistent with the assumption of laminar flow (Viskanta, 1993).

In the following results, a reference set of parameter values ($Re = 300$, $H/L = 0.75$, $B/L = 0.5$, $S/L = 0.2$, $a/L = 0.125$, $k_b/k_f = 10$ and $Pr = 0.7$) has been selected to represent a base line case. The effects of variation of jet Reynolds number, channel height, slot width, block thermal conductivity, block spacing, and block height have been investigated by changing one single parameter at a time.

5.1. Flow field

Streamline plots are used to illustrate the nature of the flow field and its dependence on the parameters of interest. The values of the stream functions (Ψ) written on top of each figure are normalized with respect to the maximum value. Positive values of Ψ represent counterclockwise flow and negative values represent clockwise flow. Twenty equal intervals are used to represent the counterclockwise flow. Five or ten levels, depending on the value of Ψ, are used to capture the vortices of the clockwise flow. To clearly delineate pertinent flow phenomena, graphical results are presented by multiplying dimensions along the y coordinate direction by a factor of approximately 3.

5.1.1. Effects of Reynolds number

Fig. 3 shows the streamline plots at three different values of Reynolds number. It can be observed that the jet enters the computational domain in the upper left corner, impinges, turns and exits at the right side of the domain. The close proximity of streamlines at the centerline of the jet near the exit port indicates the presence of jet potential core. With increasing distance from the jet inlet, the streamlines diverge as adjoining fluid is entrained within the jet. The curved streamlines at the impingement surface of the first block indicate the transition from jet to wall flow regions. As the fluid enters the system, shear forces generated at the interface between the jet and the ambient fluid induce a primary circulation zone between the jet and the confining wall. As shown in Fig. 3(a) and (b), the size

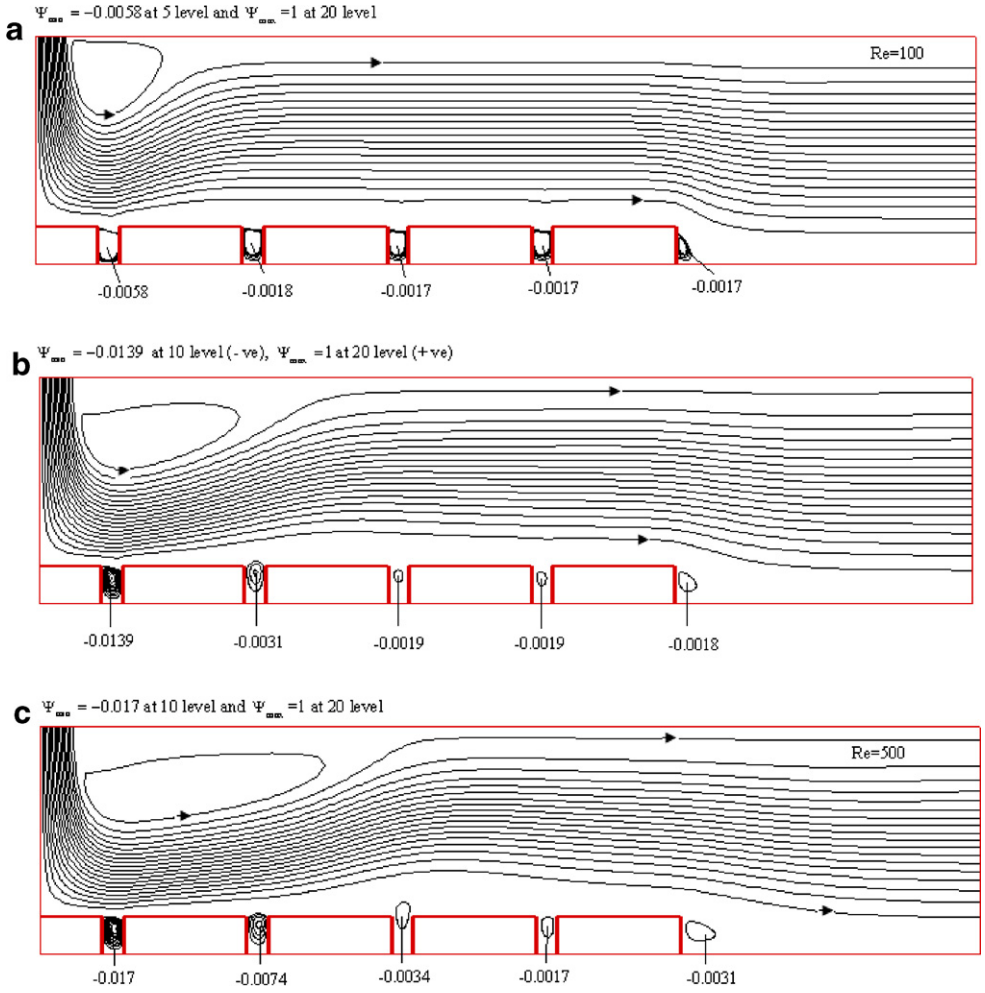

Fig. 3. Effects of Reynolds number on the flow field ($H/L = 0.75$, $B/L = 0.5$, $S/L = 0.2$, $a/L = 0.125$, $k_b/k_f = 10$ and $Pr = 0.7$): (a) $Re = 100$, (b) $Re = 300$, (c) $Re = 500$.

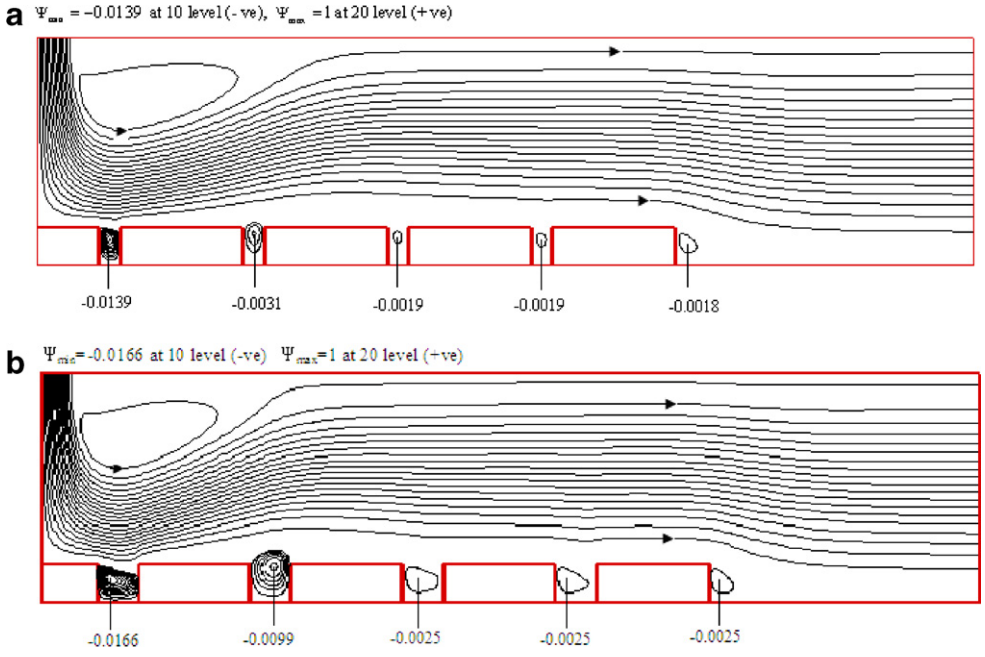

Fig. 4. Effects of block spacing S/L on the flow field ($Re = 300$, $H/L = 0.75$, $B/L = 0.5$, $a/L = 0.125$, $k_b/k_f = 10$ and $Pr = 0.7$): (a) $S/L = 0.2$, (b) $S/L = 0.4$.

and the strength of this circulation zone increases with the increase of *Re*.

Small recirculation cells are also induced in the cavities between blocks due to shear interaction between the cavity air and the main flow in the channel. The strength of the vortices formed in the cavities between blocks is relatively high between the first and the second blocks and then decreases downwards. At the downstream side of the last block, the flow is observed to separate from the impingement wall and create a weak recirculation cell. The strength of the vortices formed in the cavities between the blocks increases with increasing *Re*. This is due to the increase of the fluid forward momentum that drives the flow circulation in the cavities. It can be observed that, at high values of *Re* number, the vortices between the blocks can rise above the block top surface level, see Fig. 3(c), between the third and forth blocks. Fig. 3(a)–(c) also show that the curvature of the streamlines near the top faces of the blocks increases with increasing *Re*. The increase of the curvature of the streamlines means an increasing tendency of the flow to induce boundary layer separation at the top faces of the blocks.

The only effect of increasing block spacing S/L from 0.1 to 0.4 on the flow field is the increase of the size and strength of the vortices formed in the cavities between the blocks. This can be observed by comparing Fig. 4(a) and (b) for $S/L = 0.2$ and 0.4, respectively. However, the effects of channel height and slot width have been observed to be significant as described below.

5.1.2. Effects of channel height

The effect of the channel height H/L on the flow field is shown in Fig. 5(a)–(c) for $H/L = 0.5$, 0.75, and 1.0, respectively. It can be observed that, for values of $H/L = 0.75$ and 1.0, a circulation cell is formed between the impinging jet and the confining wall. This circulation cell increases in size with increasing H/L and observed to disappear for low values of H/L, $H/L = 0.5$. This trend is a consequence of the shear interactions at the jet/ambient interface, which becomes more influencing with increasing jet-to-plate separation distance. It can also be observed that, the tendency of flow separation and the accompanying formation of recirculation cells at the downstream blocks top surface increases with the increase of H/L. Also, the strength of

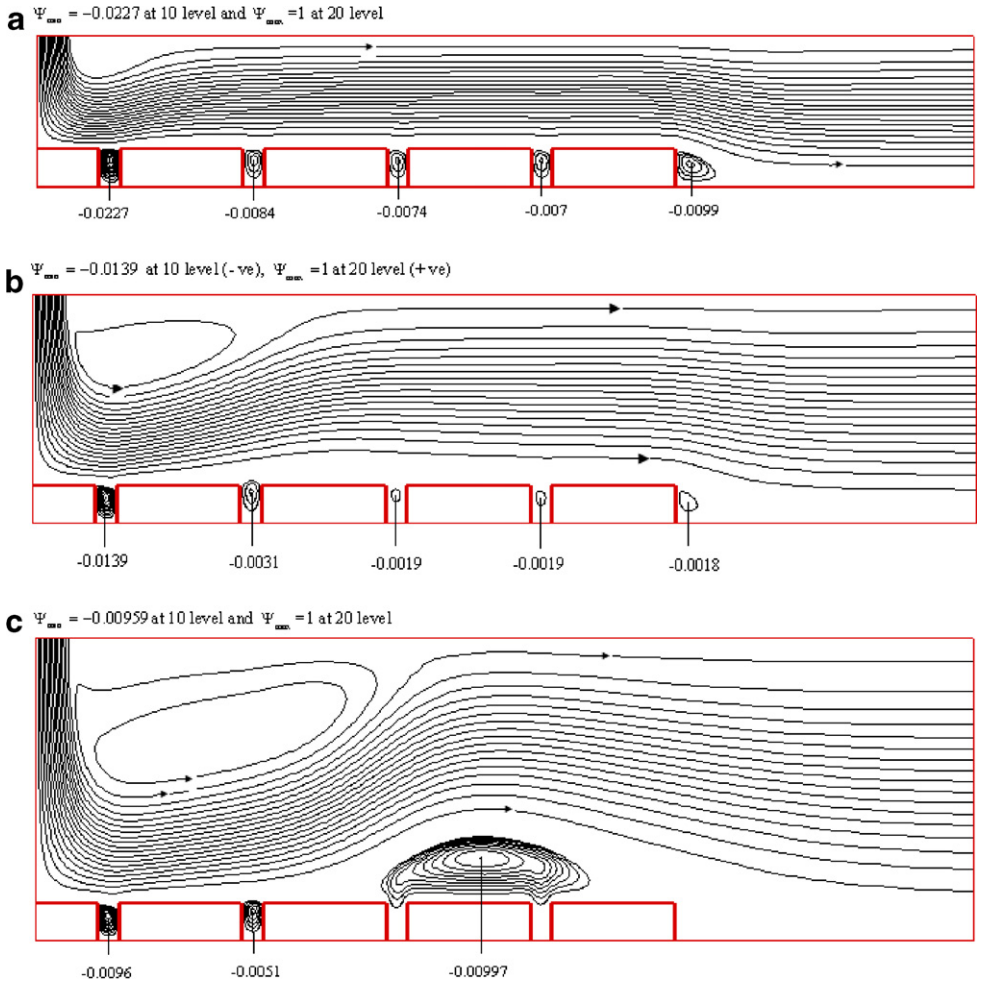

Fig. 5. Effects of channel height on the flow field ($Re = 300$, $B/L = 0.5$, $S/L = 0.2$, $a/L = 0.125$, $k_b/k_f = 10$ and $Pr = 0.7$): (a) $H/L = 0.5$, (b) $H/L = 0.75$, (c) $H/L = 1$.

the vortices formed in the cavities between the blocks decreases with increasing H/L. This is due to the decrease of the fluid forward momentum with increasing H/L. Some of these vortices may disappear with increasing H/L or decreasing Re.

5.1.3. Effects of slot width

Fig. 6(a)–(c) show the streamlines for the baseline case for slot widths $B/L = 1$, 0.5 and 0.25, respectively. As shown in Fig. 6(a), for large slot width, $B/L = 1$, no circulation cells are formed between the jet and the confining wall. Decreasing the slot width, $B/L = 0.5$ and 0.25, a circulation cell is observed to form between the jet and the confining wall and its size and strength increases with decreasing the slot width. This increase may be attributed to the increase of the jet velocity with decreasing slot width for the same Reynolds number. This circulation cell is predicted for $B/L = 0.25$ for the whole studied range of Reynolds number. For larger values of slot width, these circulation cells are predicted only at higher values of Reynolds number. The tendency of flow separation and consequent formation of recirculation cells on the top faces of the blocks increases with decreasing B/L. The position, size and strength of this vortex depend on the slot width. Decreasing the slot width shifts this vortex downstream and increases its size and strength. The strength of the vortices formed in the cavities between the blocks increases with decreasing B/L. This is due to the increase of the jet velocity and in consequence the increase of the fluid forward momentum, resulting in a larger flow circulation in the cavities between adjacent blocks. At smaller slot width, $B/L = 0.25$, and higher Reynolds number, $Re = 500$, another circulation cell was noticed downstream the heated blocks at the top confining wall.

5.2. Heat transfer

The local Nusselt number distribution around the exposed faces of the five heated blocks, for the baseline case, is shown in Fig. 7(a). Each plot shows the variation of Nu with the periphery distance x_p measured from the left bottom corner of each block as indicated on each figure. On the first block, the Nusselt number, as expected, is maximum at the jet impingement point (center of the top face

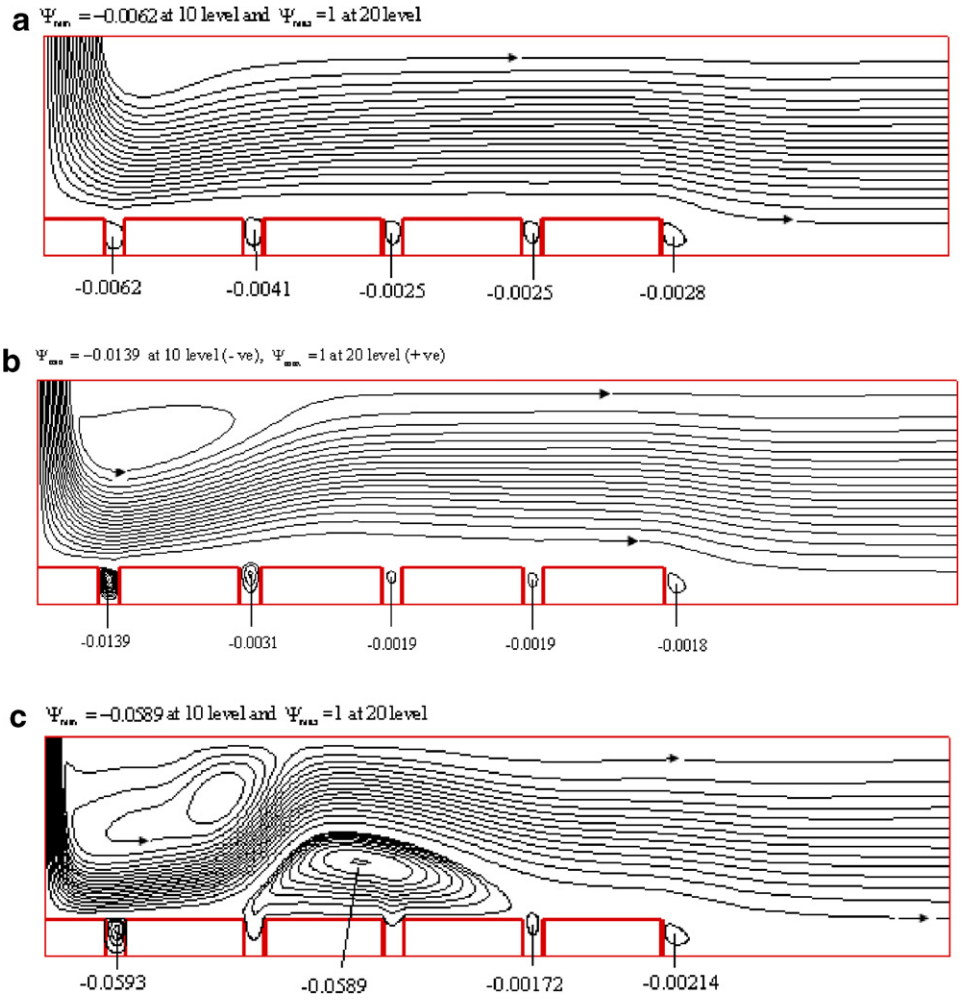

Fig. 6. Effects of slot width on the flow field ($Re = 300$, $H/L = 0.75$, $S/L = 0.2$, $a/L = 0.125$, $k_b/k_f = 10$ and $Pr = 0.7$): (a) $B/L = 1$, (b) $B/L = 0.5$, (c) $B/L = 0.25$.

of the block, $x_p = 0.025$ m), and symmetrically decreases downwards on the top and vertical faces. For blocks 2–5, the *Nu* value on the left face increases with increasing x_p ($0 < x_p < 0.005$), while it decreases with increasing x_p for the top and right faces ($0.005 < x_p < 0.045$ and $0.045 < x_p < 0.05$), respectively. At the left top corner of each block ($x_p = 0.005$) *Nu* is sharply increased due to steep velocity gradients in the flow as it turns around the blocks.

Fig. 7(b) shows the overall and surface averaged Nusselt number for the five blocks of the array. It can be observed that the mean Nusselt number on the left face, top face, and overall surface of the blocks always decreases for the downstream blocks. The opposite is true along the right faces, where the mean Nusselt number relatively increases for the downstream blocks beyond the first block. The last block in the array has the largest mean Nusselt number along its right face. This can be explained as due to the absence of upstream conduction heat transfer from adjoining downstream blocks and the presence of downstream recirculation cell that relatively augments the heat transfer rate from the last block right face. The mean Nusselt number along the top face of any block of the array is higher than those along its right and vertical faces. This can be attributed to the relatively high convective heat transfer from top surfaces to the low temperature axial core flow.

Thermal transport in the inter-spaces between blocks is controlled by two mechanisms: convective heat exchange with the axial core flow as due to weak re-circulating flow in the top region and upstream conduction in the stagnant bottom region. At low values of *Re* and *S*/*L*, heat conduction in the bottom region is dominant and results in negative *Nu* values on the right faces of the upstream blocks, see Fig. 7(a). These negative *Nu* values indicate that this portion of the face is heated and not cooled. At high values of *Re* and *S*/*L* and low values of *a*/*L*, the size and intensity of re-circulating flow in the cavity space between adjacent blocks increase and eliminate upstream heat conduction within these spaces. Therefore, the values of *Nu* on the right faces of the upstream blocks of the cavity are always positive.

Also, Fig. 7(b) shows that the mean Nusselt number along different faces of the blocks and the overall mean Nusselt number for the whole exposed surface of the blocks are approximately equal for the forth and fifth blocks. The difference in values between block 4 and 5 is within 4%. Excluding the block under the jet, the present trend of variation of the mean Nusselt number with block number is similar to the previous numerical results of Young and Vafai (1998) for parallel channel flow over heated blocks where the mean Nusselt number has been found to be row independent after the third row.

5.2.1. Effects of Reynolds number

The effects of Reynolds number on both the local Nusselt number distribution and the mean Nusselt number around the exposed faces of the five heated blocks of the array are shown in Fig. 8(a)–(f). In general, increasing *Re* increases the local Nusselt number on the top face of each block of the array. This is due to the reduction in the thermal boundary layer thickness on the top faces of the blocks with the increase of the Reynolds numbers. However, Fig. 8(d) for block 4 shows that the increase of *Re* value from 400 to 500 decreases the local Nusselt number on the top face of this block. This can be attributed to the tendency of the flow to induce boundary layer separation at the top face of this block. This tendency of the separation deflects the flow away from the top face of the block and reduces the heat transfer rates. Also, Fig. 8(a)–(e) shows the increase of the local Nusselt number on the left faces of the blocks with the increase of the Reynolds number. This is due to the increase of the strength of the vortices formed in the cavities between the blocks. There is no general trend for the effect of Reynolds number on the mean Nusselt number of the right faces of the blocks. This can be attributed as due to the counteracting mechanisms of heat transfer modes from this face. Increasing the Reynolds

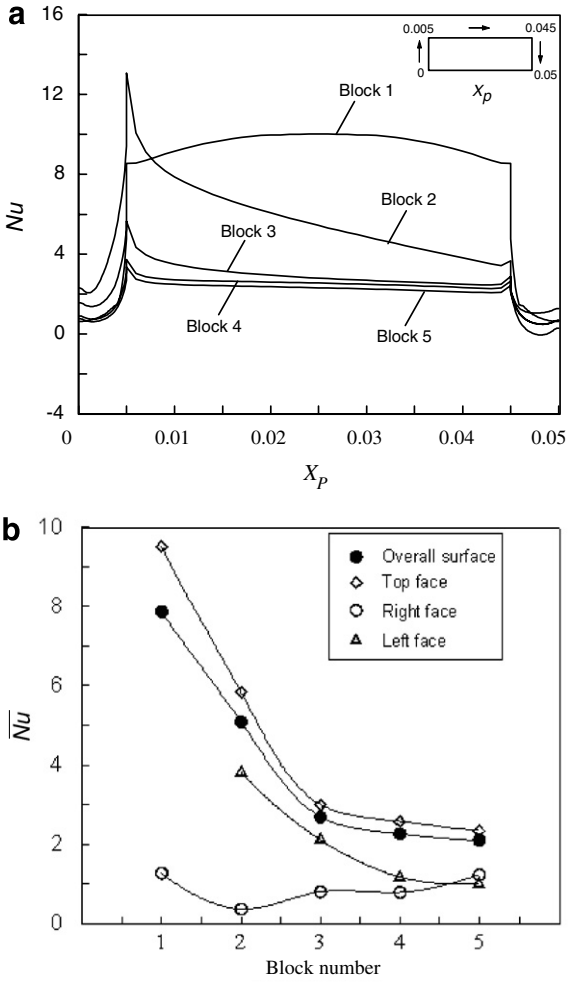

Fig. 7. Heat transfer characteristics for the baseline case ($Re = 300$, $H/L = 0.75$, $B/L = 0.5$, $S/L = 0.2$, $a/L = 0.125$, $k_b/k_f = 10$ and $Pr = 0.7$): (a) local Nusselt number along the block periphery, (b) overall and surface averaged Nusselt number.

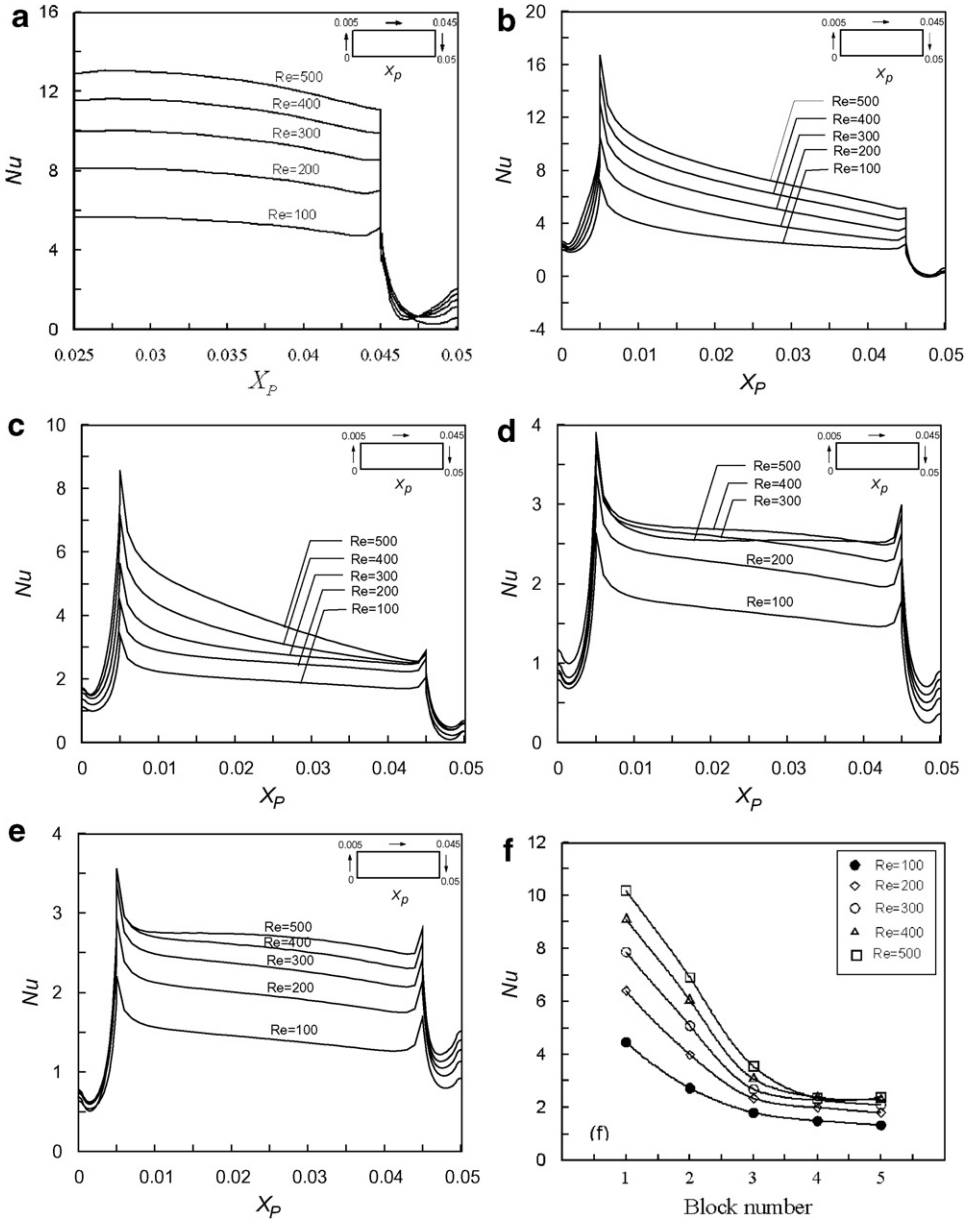

Fig. 8. Effects of Reynolds number on the heat transfer characteristics ($H/L = 0.75$, $B/L = 0.5$, $S/L = 0.2$, $a/L = 0.125$, $k_b/k_f = 10$ and $Pr = 0.7$): (a)–(e) local Nusselt number distribution along the block periphery, (f) overall mean Nusselt number.

number increases the strength of the vortices in the cavities and increases the convective cooling rate of the right face. However, these vortices may rise upwards and increase the conduction zone at the bottom of the cavity with increased upstream negative (heating effect) heat transfer. In general, Fig. 8(f) shows the increase of the overall mean Nusselt number around the entire exposed surface of the blocks with the increase of the Reynolds number.

5.2.2. Effects of channel height

The effects of H/L on the heat transfer characteristics are shown in Fig. 9(a)–(e). Higher values of heat transfer rates are obtained at values of $H/L = 0.5$. At higher values of H/L ($H/L = 0.75$ and 1.0), recirculation cells developed on the top faces of downstream blocks change dramatically the heat transfer rates from these blocks. Normally, one may expect a decrease in the Nusselt number value on the top faces of downstream blocks of the array with the increase of H/L as due to the decrease of the core flow velocity. However, as can be seen in Figs. 9(a)–8(e), the formation of a recirculation cell at $H/L = 1.0$ on the top surface of the forth block leads to the increase of the local Nusselt number value at both the trailing edge of the second block and the leading edge of the third block, respectively. While the local Nusselt number values on the other portions of the top surfaces of these blocks and blocks 1, 4 and 5 are observed to decrease. Also, Figs. 9(a)–8(e) show the decrease of the local Nusselt number on the left and

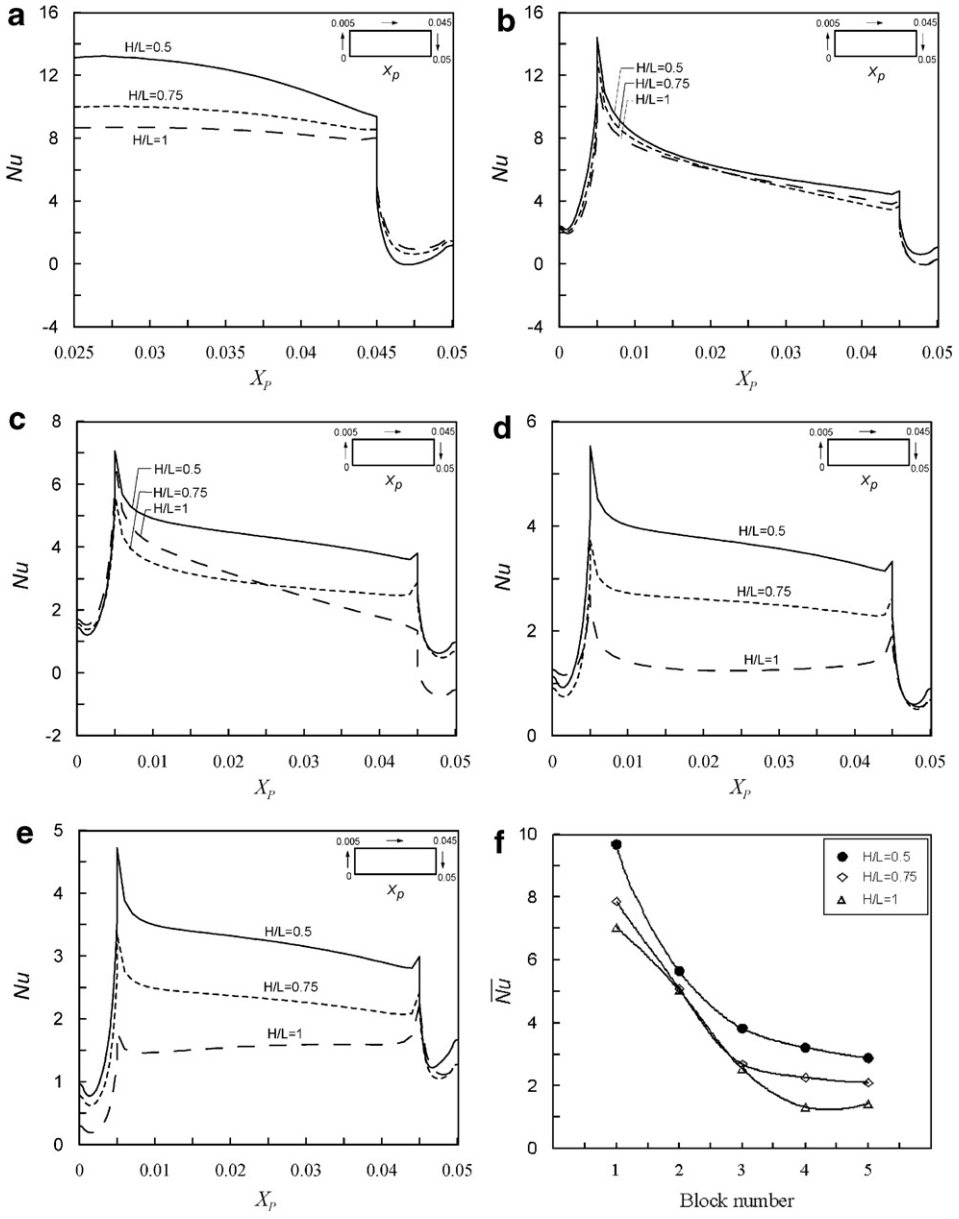

Fig. 9. Effects of H/L on the heat transfer characteristics ($Re = 300$, $B/L = 0.5$, $S/L = 0.2$, $a/L = 0.125$, $k_b/k_f = 10$ and $Pr = 0.7$): (a)–(e) local Nusselt number distribution along the block periphery, (f) overall mean Nusselt number.

right faces of the blocks of the array, except the right face of the first block, with the increase of H/L. This is due to the decrease of the strength of the vortices formed in the cavities between the blocks.

Fig. 9(f) shows the decrease of the overall mean Nusselt number along the entire exposed surface of the blocks with the increase of H/L. This is due to the lower jet impact velocity and weaker core flow at high values of H/L. However, increasing H/L to a range where vortices are formed on the top faces of some blocks of the array may lead to the increase or decrease of the mean Nusselt numbers of these blocks of the array. This effect is shown in Fig. 9(f) where the mean Nusselt number for blocks 2 and 3 are approximately equal for H/L 0.75 and 1.5. For lower values of Re ($Re = 100$ and 200), where the recirculation cell on the surface of the blocks does not appears, the mean Nusselt number on all the blocks of the array decreases with increasing H/L.

5.2.3. Effects of slot width

The effects of the slot width on both the local Nusselt number distribution and the mean Nusselt number around the exposed faces of the five heated blocks, for the baseline case are shown in Fig. 10(a)–(f) for $B/L = 0.25$, 0.5 and 1. It can be observed that, for upstream blocks, blocks 1 and 2, the Nusselt number values increase with the decrease of B/L. This can be attributed to the increase of velocity gradient at the faces of these blocks with the increase of jet velocity. The primary circulation cell acts to confine the wall jet flow region and inhibits flow expansion and

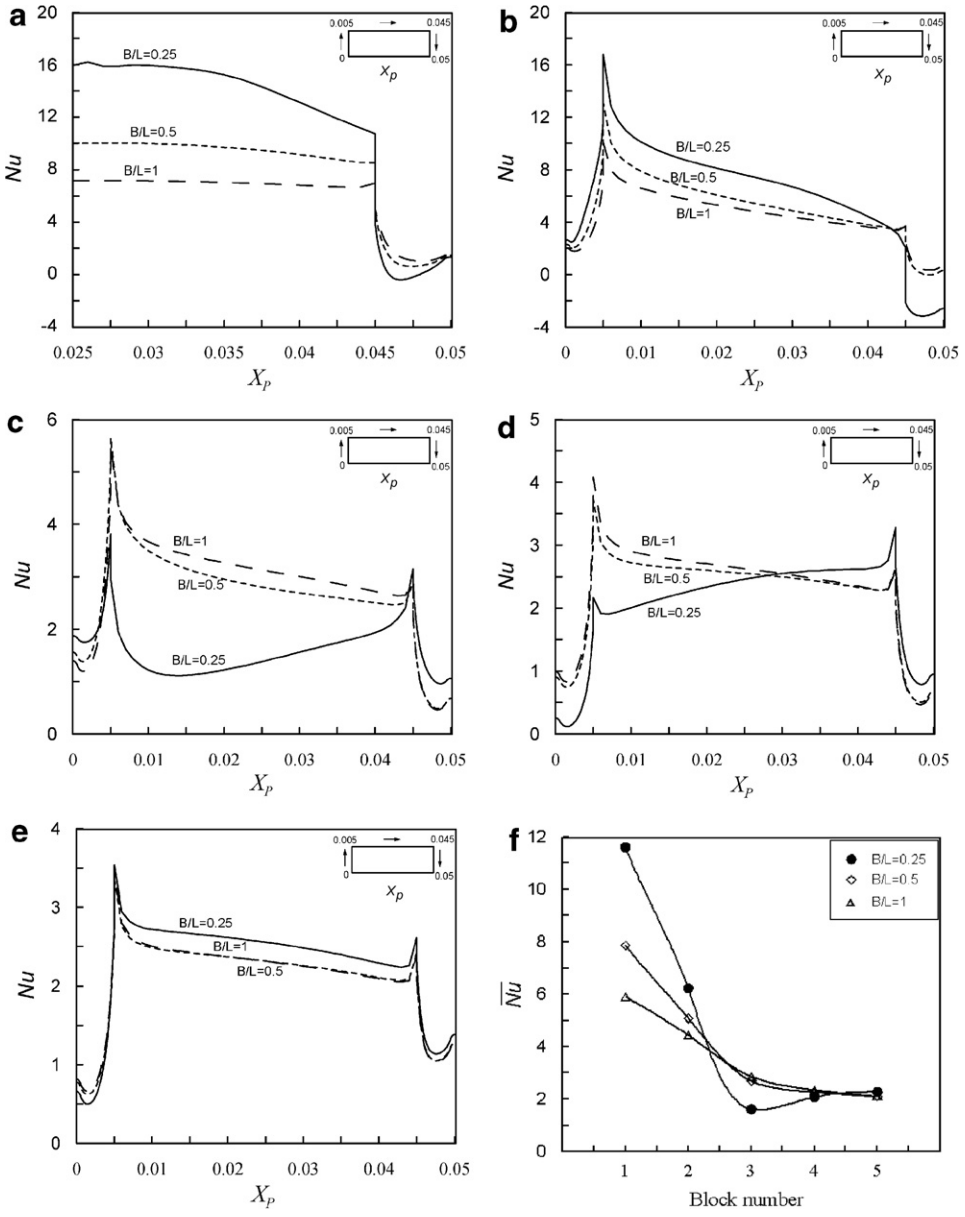

Fig. 10. Effects of B/L on the heat transfer characteristics ($Re = 300$, $H/L = 0.75$, $S/L = 0.2$, $a/L = 0.125$, $k_b/k_f = 10$ and $Pr = 0.7$): (a)–(e) local Nusselt number distribution along the block periphery, (f) overall mean Nusselt number.

separation. On the other hand, the Nusselt number values for Blocks 3 and 4, see Fig. 10(c) and (d), are adversely affected with the decrease of B/L as due to the formation of secondary recirculation cell on the top surfaces of these blocks. In fact, the formation of this recirculation cell is function of values of Re, H/L, and B/L as explained before. Fig. 10(f) shows an increase in $\overline{Nu}$ values for blocks 1 and 2 and a decrease in $\overline{Nu}$ value for block 3 with the decrease of B/L.

5.2.4. Effects of block thermal conductivity

The local Nusselt number distribution around the five blocks of the array for the baseline case with $k_b/k_f = 10$, 100 and 1000 is shown in Fig. 11(a)–(e). It can be observed that the local Nusselt number along the top and right faces decreases with increasing k_b/k_a from 10 to 100. Along the left faces, the local Nusselt number slightly increases with the increase of k_b/k_a from 10 to 100. It is interesting to note that increasing k_b/k_f from 10 to 100 then from 100 to 1000 sharply increases the local Nusselt number near the upper left corners of the blocks and slightly decreases it near the upper right corners. Heat transfer rates at these corners are controlled by the intensity of convection currents that are relatively higher near the upper left corners of the blocks. This can be explained by considering a two-dimensional control volume around these corners which shows that the ratio of convective surface area to solid (conductive) mass is twice that of a surface point away from the corners. Also, Figs. 11(a)–(e) reveal that increasing k_b/k_f from 100 to 1000 has no effect on the local Nusselt number

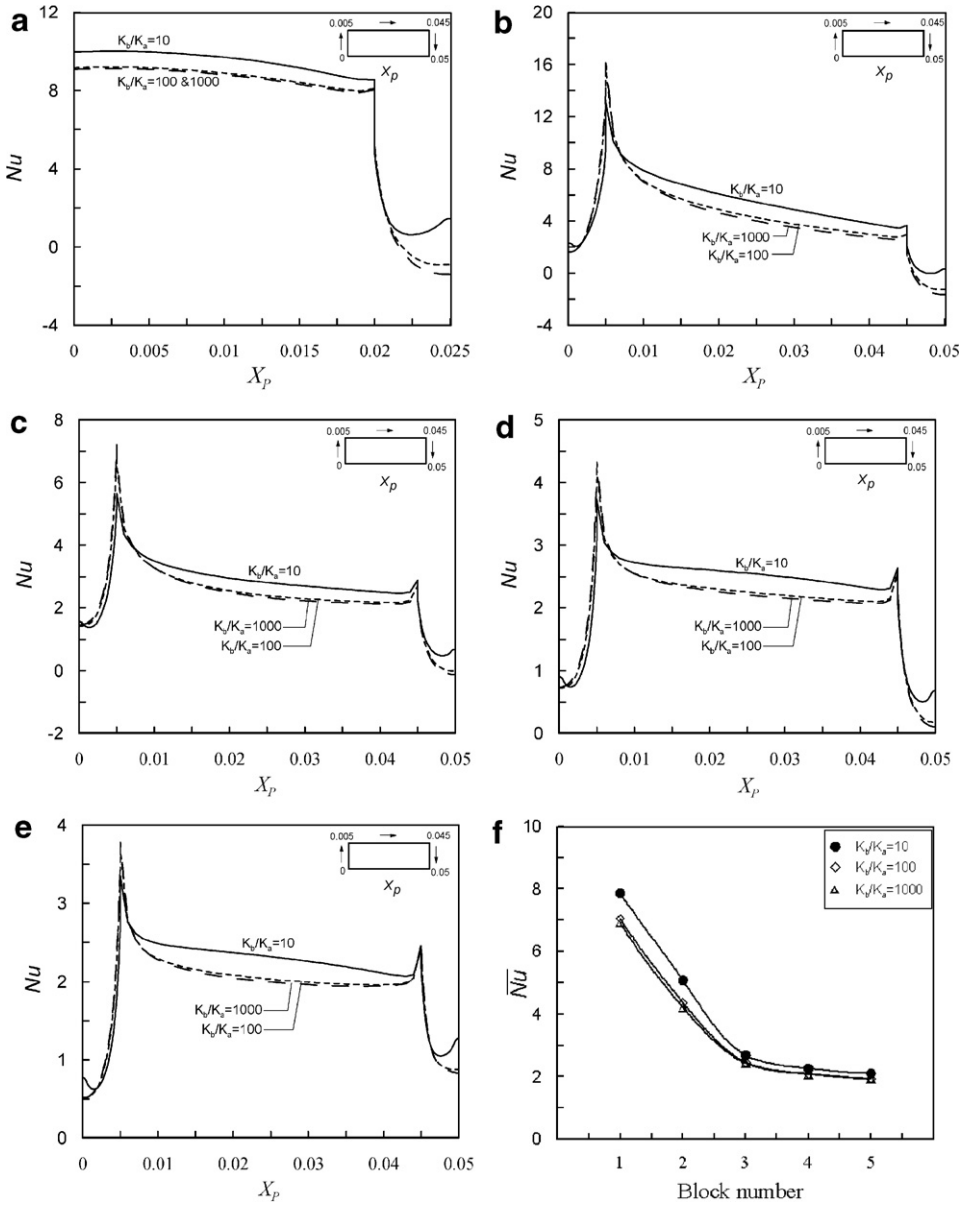

Fig. 11. Effects of k_b/k_a on the heat transfer characteristics ($Re = 300$, $B/L = 0.5$, $H/L = 0.75$, $S/L = 0.2$, $a/L = 0.125$, and $Pr = 0.7$): (a)–(e) local Nusselt number distribution along the block periphery, (f) overall mean Nusselt number.

distributions. The present results are in accordance with the findings of Young and Vafai (1998) for heated blocks in parallel flow.

Fig. 11(f) shows that increasing k_b/k_f from 10 to 100 reduces the mean Nusselt number around the blocks of the array. The amount of this reduction in mean Nu value is significant for the first and second blocks and decreases for the downstream ones. The decrease of mean *Nu* value with the increase of k_b/k_f should be carefully interpreted. Since the *Nu* value represents the ratio between convective and conductive heat transfer rates, the decrease in *Nu* value with the increase of k_b/k_f may be attributed to higher rates of increase of conductive heat transfer rate and not to low convective ones. Therefore, one should also examine the temperature distribution along the exposed block surfaces to asses the variation of effective cooling of blocks with the increase of k_b/k_f. As shown in Fig. 12, for all blocks, the block temperature becomes nearly isothermal for high values of k_b/k_f. For the first and second blocks, the mean block temperature decreases with the increase of k_b/k_f. These observations indicate a general enhancement of cooling effectiveness with increasing k_b/k_f value.

5.2.5. Effects of block spacing

As mentioned before, the only effect of increasing S/L from 0.1 to 0.4 on the flow field is the increase of the size and strength of the vortices formed in the cavities between the blocks. Increasing the strength of these vortices leads to the increase of the local Nusselt number on the left and right faces of each block of the array as shown in

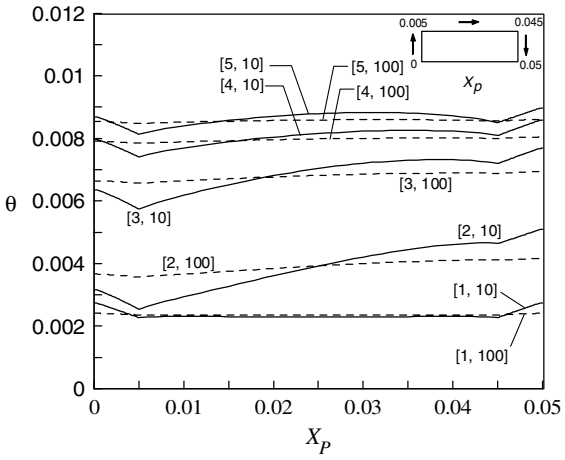

Fig. 12. Variation of block wall temperature with k_p/k_f ($Re = 300$, $B/L = 0.5$, $H/L = 0.75$, $S/L = 0.2$, $a/L = 0.125$, and $Pr = 0.7$), Key: [block number, k_b/k_f].

Fig. 13(a)–(e). Along the top faces, Fig. 13(a) shows that increasing S/L has no effect on the local Nusselt number on the top face of block number 1 because the position of the first block with respect to the jet does not change with changing S/L. Fig. 13(b) and (c) show that there is a slight decrease in the local Nusselt number for blocks number 2 and 3 with increasing S/L. This decrease is due to the displacement of these blocks, which lie within the impingement flow region, away from the impinging jet stagnation point with increasing S/L. On the other hand, increasing S/L slightly increases the local Nusselt number on the top faces of blocks number 4 and 5 that already lies in the wall jet region. As the spacing between these blocks increases, there is a greater dissipation of the thermal boundary layer downstream of the trailing edge of one block and hence a less developed boundary layer at the leading edge of the next block. A larger spacing between these blocks therefore results in larger local heat transfer coefficient on the top faces of these blocks. This variation of the local Nusselt number distributions for different blocks of the array with S/L gives: (a) slight increase in the mean Nusselt number around the exposed surfaces of blocks 1, 4 and 5 with increasing S/L, and (b) no variation in the mean Nusselt number around the exposed surfaces of blocks 2 and 3 with increasing S/L, as shown in Fig. 13(f).

5.2.6. Effects of block height

Fig. 14(a)–(e) show the increase of the local Nusselt number along the top faces of the five blocks of the array with the increase of block height. This is due to the increase of the core flow velocity as the core flow region becomes thinner with increasing block height. However, increasing the block height decreases the local Nusselt number along the left and right faces of blocks and increases the portions of block right face that are characterized by negative values of local Nusselt number. This can be attributed to the decrease of the strength of the vortices in the cavities between blocks with increasing block height and the reduction of its interaction and mixing with the core flow. Moreover, increasing the block height increases the conduction zone at the bottom of the cavities which leads to upstream heat transfer. These counter acting mechanisms of enhancement and decrease of heat transfer rates from different block faces with the increase of block height are summarized in the variation of overall surface averaged Nusselt number with Block number shown in Fig. 14(f) which indicates an overall decrease in $\overline{Nu}$ value for blocks 1 and 2 and negligible change for other downstream blocks with the increase of block height.

5.2.7. Effects of jet velocity profile

In the above results, a uniform velocity profiles is assumed for the jet velocity at the slot exit. The effects of exit jet velocity profile on the local heat transfer rates from the blocks is shown in Fig. 15 where results are presented for both uniform and fully developed parabolic velocity profiles with the same mean velocity value at the jet discharge. It can be observed from Fig. 15(a) that the stagnation line heat transfer Nusselt number is higher for the parabolic profile. Using a uniform velocity profile, the heat transfer distribution of Block 1 is more uniform. This can be explained as due to the larger midline velocity for the fully developed jet. Also, it is observed that, the jet entrains more fluid and, therefore, spreads further with a uniform velocity profile at the nozzle exit. This is attributed as due to the existence of larger shear forces at the jet/ambient interface for the uniform velocity profile than for the fully developed profile, which is characterized by an initial interface velocity of zero. The shape of local heat transfer distribution from the downstream blocks is not affected by the velocity profiles. However, using a parabolic profile, the overall and top surface averaged heat transfer Nusselt numbers are relatively higher, see Fig. 15(b). The left and right face averaged values of Nusselt number are slightly dependent on the velocity profile. One should mention here that, due to compact space limitations in electronics applications, the slot length is very small and the assumption of a uniform velocity profile at the jet exit is close to reality.

6. Useful correlations

Efficient cooling of electronic equipment is the aim of design engineers to handle the expected high rates of heat dissipation and avoid working at high operating temperature which decreases the reliability and performance and may lead to potential failure of the electronic equipment. Quantitative information for the average Nusselt number for different blocks of the array of multiple heat sources simulating electronic equipment are needed to predict the average temperatures of any block of the array. Therefore, it would be useful to formulate the present numerical results to provide design correlations in terms of the controlling parameters.

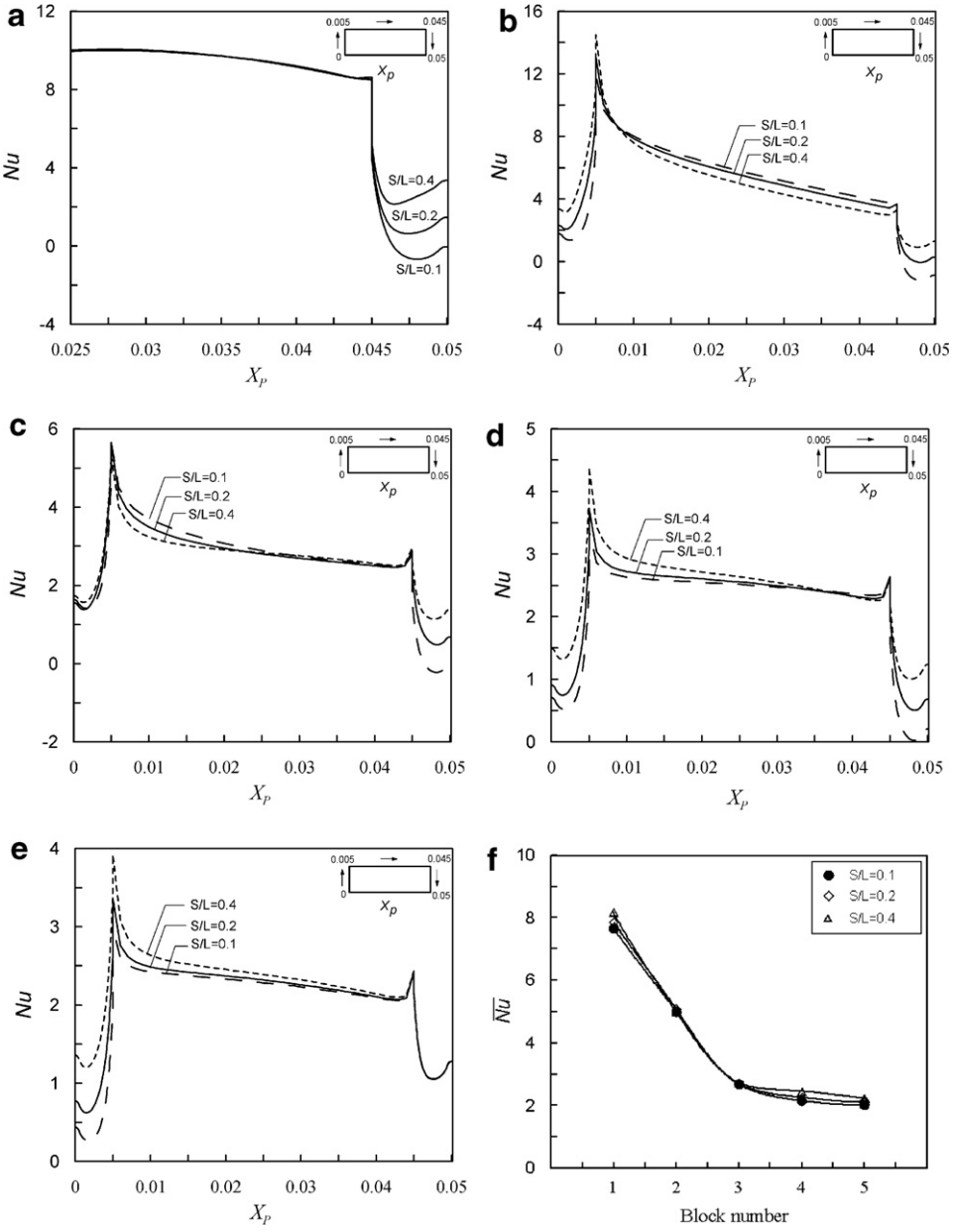

Fig. 13. Effects of block spacing on the heat transfer characteristics ($Re = 300$, $B/L = 0.5$, $H/L = 0.75$, $a/L = 0.125$, $k_b/k_f = 10$, and $Pr = 0.7$): (a)–(e) local Nusselt number distribution along the block periphery, (f) overall mean Nusselt number.

The presence, disappearance, and the position of the vortices that are observed to form on the top surfaces of some blocks of the array remarkably change the mean Nusselt number of these blocks. This leads to the difficulty of correlating the present data by a single correlation giving the mean Nusselt number at any blocks of the array in terms of the controlling parameters (Re, H/L, B/L and a/L). However, careful examination of the present results shows that these vortices are formed only on the third block and sometimes on the trailing edge of the second block. For the third block, these recirculation vortices are only noticed to form at low values of slot widths ($B/L \leqslant 0.25$). Regression analysis of the present data result in the following heat transfer correlations for the overall average Nusselt number for heat transfer from each block of the array (Nu_n, where n refers to the block number):

$$\overline{Nu}_1 = 0.207Re^{0.53}(H/L)^{-0.452}(B/L)^{-0.49}(a/L)^{-0.07} \quad (8)$$

$$\overline{Nu}_2 = 0.18Re^{0.53}(H/L)^{-0.152}(B/L)^{-0.19}(a/L)^{-0.07} \quad (9)$$

$$\overline{Nu}_3 = 0.093Re^{0.53}(H/L)^{-0.552}(B/L)^{-0.59}(a/L)^{-0.07} \quad \text{for } B/L \geqslant 0.5 \quad (10)$$

$$\overline{Nu}_3 = 0.107Re^{0.53}(H/L)^{-0.552}(2B/L)^{-0.49+0.004Re}(a/L)^{-0.07} \quad \text{for } B/L \leqslant 0.25 \quad (11)$$

$$\overline{Nu}_{4,5} = 0.213Re^{0.34}(H/L)^{-0.97} \quad (12)$$

These correlations are valid for the range of parameters evaluated in the present study ($Re = 100$–500,

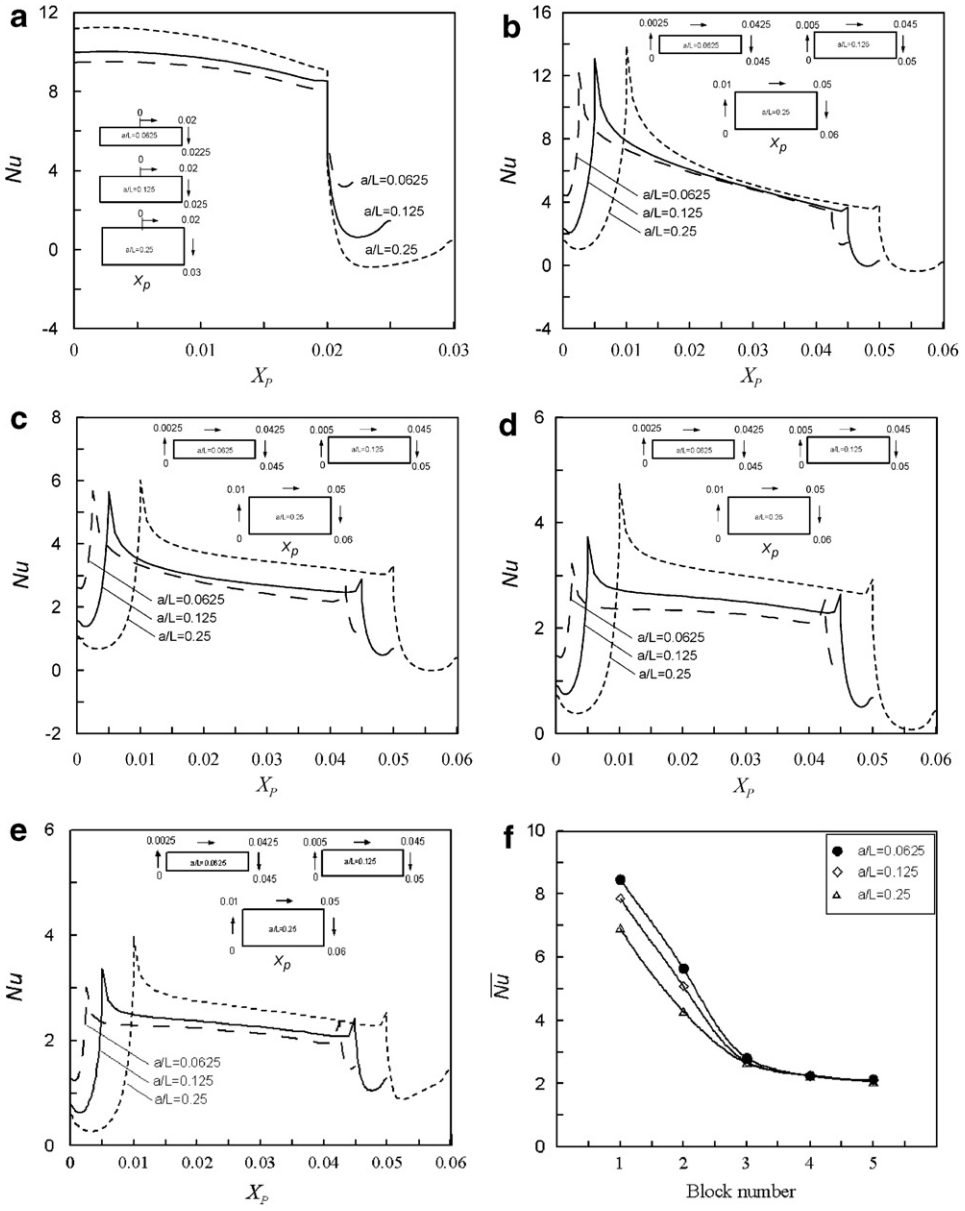

Fig. 14. Effects of block height on the heat transfer characteristics ($Re = 300$, $B/L = 0.5$, $H/L = 0.75$, $S/L = 0.2$, $k_b/k_f = 10$, and $Pr = 0.7$): (a)–(e) local Nusselt number distribution along the block periphery, (f) overall mean Nusselt number.

$H/L = 0.5$–1, $B/L = 0.25$–1, $a/L = 0.0627$–0.25, $Pr = 0.7$ and k_b/k_f). It should be observed that, two correlating equations have been developed for the third block for $B/L \geqslant 0.5$ and $B/L \leqslant 0.25$, corresponding respectively to the conditions of absence and presence of vortices above this block. Eqs. (8)–(12) predict all the data of the mean Nusselt number around the surface of any block of the array within ±15%.

7. Summary and conclusions

The present study is motivated by the utilization of a laminar slot jet to cool a linear array of protruding discrete heat sources in electronics cooling applications. A comprehensive numerical investigation of fluid flow and heat transfer characteristics have been carried out for different values of jet Reynolds number, channel height, slot width, spacing between blocks, block height, and block thermal conductivity. The effects of variation of these parameters are detailed to illustrate important fundamental and practical results.

In general, the flow field is characterized by the existence of impingement flow and wall jet flow regions in addition to the possible existence of a primary circulation cell between the impingement jet and the confining wall, secondary circulation cells between the blocks, and a secondary recirculation cell at the top surface of downstream blocks. The size and the strength of primary circulation cell, the strength of secondary circulation cells between the blocks, and the tendency of flow separation and the

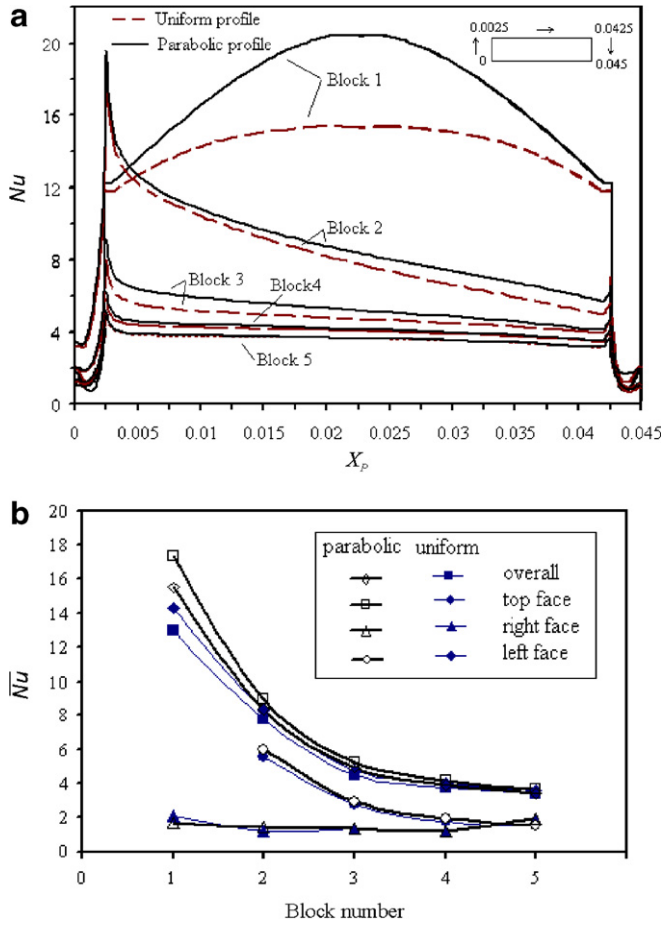

Fig. 15. Effects of velocity profile on the heat transfer characteristics ($Re = 500$, $H/L = 0.5$, $B/L = 0.5$, $S/L = 0.1$, $a/L = 0.0625$, $k_b/k_f = 10$ and $Pr = 0.7$): (a) local Nusselt number along the block periphery, (b) overall and surface averaged Nusselt number.

accompanying formation of recirculation cells at the downstream blocks top surface increase with the increase of Re and H/L and the decrease of B/L. The existing flow structure is found to significantly influence the corresponding heat transfer characteristics.

In general, the cooling effectiveness for all the blocks increases with increasing Reynolds number and decreasing slot width and channel height. Narrow gaps between relatively tall blocks are found to augment upstream heat conduction and consequent heating of the right face of the upstream blocks, in particular at low values of Reynolds number. Shorter and widely spaced heated blocks are found to produce more effective cooling. Increasing Reynolds number and channel height and decreasing slot width and block height may lead to the formation of recirculation cells on the top surface of the downstream blocks that dramatically decreases the heat transfer rates from these blocks. Large values of block thermal conductivity decrease and homogenize the block temperature. The local distribution of Nusselt number along the periphery of Blocks indicates relatively low rates of heat transfer from the block right face as compared to other faces.

Analysis of the mean values of Nusselt number has shown that the block just underneath the air jet has the maximum mean Nusselt number and the Nusselt number decreases for the downstream blocks until it reaches approximately constant value after the third block. In general, for the range of parameters studied, the block mean Nusselt number increases with the increase of Reynolds number, decrease of channel and block height. Its variation with slot width is not monotonic and the effect of block spacing is marginal. Useful design correlations have been obtained for the mean Nusselt number for the heat sources underneath and downstream the impinging jet.

Acknowledgement

The present work has been carried out in the framework of scientific cooperation between TREFLE and BHIT. The financial support of University of Bordeaux 1 and TREFLE for S.A. Nada during his stay at TREFLE is highly appreciated.

References

Angot, P., Bruneau, C.-H., Fabrie, P., 1999. A penalization method to take into account obstacles in viscous flows. Numer. Math. 81, 497–520.

Aquilon, 2006. Outil de modelisation en mecanique des fluids et transferts, TREFLE-ENSCPB, http://www.trefle.u-bordeaux1.fr/index.html.

Arquis, E., Caltagirone, J.-P., 1984. Sur les conditions hydrodynamiques au voisinage d'une interface milieu fluide—milieu poreux—application à la convection naturelle, C. R. Acad. Sci. 299 (II), 1–4.

Behnia, M., Parneix, S., Shabany, Y., Durbin, P.A., 1999. Numerical study of turbulent heat transfer in confined and unconfined impinging jets. Int. J. Heat Fluid Flow 20, 1–9.

Bula, A.J., Rahman, M.M., Leland, J.E., 2000. Axial steady free surface jet impinging over a flat disc with discrete heat sources. Int. J. Heat and Fluid flow 21, 11–12.

Fortin, M., Glowinski, R. 1982. Methode de la Lagrangien Augmente. Application a La Resolution Numerique des Problemes aux Limites. In: Collection Methodes Mathematiques de l' Informatique, Dunod, Paris.

Hollworth, B.R., Durbin, M., 1992. Impingement cooling of electronics. ASME J. Heat Transfer 114, 607–613.

Huzyyien, A.S., Nada, S.A., Rady, M.A., Faris, A., 2006. Cooling an array of multiple heat sources by a row of slot air jets. Int. J. Heat and Mass Transfer 49, 2597–2609.

Incropera, F.P., 1988. Convection heat transfer in electronic equipment cooling. J. Heat Transfer 110, 1097–1111.

Jambunathan, K., Lia, E., Moss, M.A., Button, B.L., 1992. A review of heat transfer data for single circular jet impingement. Int. J. Heat Fluid Flow 13, 106–115.

Khadra, K., Angot, P., Parneix, S., Caltagirone, J.-P., 2000. Fictitious domain approach for numerical modeling of Navier–Stokes equations. Int. J. Numer. Methods Fluids 34, 651–684.

Kim, S.J., Lee, S.W., 1996. Air Cooling Technology for Electronic Equipment. CRC Press, New York.

Lin, Z.H., Chou, Y.J., Hung, Y.H., 1997. Heat transfer behaviors of a confined slot jet impingement. Int. J. Heat Mass Transfer 40, 1095–1107.

Mesbah, M.P.E., 1996. An experimental study of local heat transfer to an impinging jet on non-flat surfaces: a cylindrical pedestal and a hemi spherically concave surface. Ph.D. Thesis, University of California, Davis.

Patankar, S.V., 1980. Numerical Heat Transfer and Fluid Flow. Hemisphere/McGraw-Hill, Washington.

Peterson, G.P., Ortega, A., 1990, Thermal control of electronic equipment and devices. In: Hartnett, J.P., Irvine, T.F. (Eds.), Advances in Heat Transfer, vol. 20, pp. 181–314.

Plot, S., Huang, B., Mujumdar, A.S., Douglas, W.J.M., 1989. Numerical flow and heat transfer under impinging jets: a review. Annual Rev. Numer. Fluid Mech. Heat Transfer 2, 157–159.

Schafer, D.M., Ramadhyani, S., Incropera, F.P., 1992. Numerical simulation of laminar convection heat transfer from an in-line array of discrete sources to a confined rectangular jet. Numer. Heat Transfer 22 (Part A), 121–141.

Sparrow, E.M., Wong, T.C., 1975. Impingement transfer due to initially laminar slot jets. Int. J. Heat Mass Transfer 18, 597–605.

Viskanta, R., 1993. Heat transfer to impinging isothermal gas and flame jets. Exp. Thermal Fluid Sci. 6, 111–134.

Wadsworth, D.C., Mudawar, I., 1990. Cooling of multiple electronic modules by means of confined two-dimensional jets of dielectric liquid. Int. J. Heat Mass Transfer 112, 891–898.

Yeh, L.T., 1995. Review of heat transfer technology in electronic equipment. J. Electron. Packaging 117, 333–339.

Young, T.J., Vafai, K., 1998. Convective flow and heat transfer in a channel containing multiple heated obstacles. Int. J. Heat Mass Transfer 41, 3279–3298.